CrystEngComm

RSC Publishing

COMMUNICATION

View Article Online
View Journal | View Issue

Template-free synthesis and gas sensing properties of hierarchical hollow ZnO microspheres†

Cite this: *CrystEngComm*, 2013, **15**, 7438

Received 8th May 2013,
Accepted 25th July 2013

DOI: 10.1039/c3ce40812d

www.rsc.org/crystengcomm

Dawei Wang,[a] Sisi Du,[a] Xin Zhou,[a] Biao Wang,[b] Jian Ma,[a] Peng Sun,*[a] Yanfeng Sun[a] and Geyu Lu*[a]

Hierarchical hollow ZnO microspheres were prepared *via* a one-pot template-free hydrothermal synthesis. It's worth mentioning that the hollowness of these microspheres could be controlled by adjusting the zinc source concentration. Furthermore, these microspheres were integrated into a sensorial structure which exhibited fast response and recovery times and good selectivity to ethanol.

Hierarchical structures, as a higher dimension of micro- and nanostructures assembled from low dimensional blocks, such as zero-dimension (0D) nanoparticles, nanowires (1D), nanorods (1D), nanotubes (1D) and nanosheets (2D),[1] have become a research hotspot due to its peculiar characteristics. At the same time, hollow structures have also attracted intensive attention in the past few decades because of their low density and well-defined morphologies.[2] ZnO, as an n-type semiconductor material with a wide band gap (3.37 eV) and large excitation binding energy (60 meV),[3] has been prepared with different hierarchical hollow structures. Saito *et al.* presented a topical review on the hierarchical structures of ZnO spherical particles synthesized using a mixture of ethylene glycol (EG) and water as the solvent.[4] Wang *et al.* prepared ZnO spheres composed of porous flakes by annealing the precursor.[5] Wang *et al.* reported aggregation-induced growth of hexagonal ZnO hierarchical mesocrystals with an interior space.[6]

As a functional material, ZnO has been extensively studied in various applications.[7–12] One of the most important applications of ZnO material is in gas senors due to its typical properties, such as high electrochemical stability, absence of toxicity and abundance in nature.[13] Recently, ZnO has been developed with various morphologies and structures for gas sensors. Lupan *et al.* built a highly sensitive and selective hydrogen sensor using cadmium-doped ZnO nanowires.[14] Zhang *et al.* reported the NH_3 and NO_2 gas sensing properties of ZnO hollow spheres, which were prepared by using carbon microspheres as templates.[15] Tian *et al.* prepared ZnO hollow microspheres *via* a precursor–template thermal evaporation method, which were used for detecting ethanol.[16] In this work, hierarchical hollow ZnO microspheres were prepared by a one-pot hydrothermal method without any templates. To the best of our knowledge, such novel ZnO architectures obtained *via* a simple method and used for gas sensors have been rarely reported. Interestingly, the interior structure of these ZnO microspheres could be adjusted by varying the zinc source concentration. In order to understand the formation mechanism of these microspheres, a series of experiments depending on different reaction times were performed. For the potential applications, these hierarchical hollow microspheres exhibited an excellent gas sensing performance to ethanol.

Fig. 1(a) shows the typical X-ray diffraction (XRD) pattern of the product obtained at the zinc acetate concentration of 0.05 M (see ESI† for experimental details). All of the diffraction peaks can be indexed to the hexagonal ZnO structure (JCPDS No. 36-1451). No diffraction peaks of any other impurities were observed, which indicates the good purity of the products. The morphology and structure of the as-prepared products were observed by field emission scanning electron microscopy (FESEM) and transmission electron microscope (TEM). The low magnification of FESEM image in Fig. 1(b) shows that the products consists of monodisperse and uniform ZnO microspheres with diameters of 3–4 μm. The high magnification FESEM images in Fig. 1(c) and (d) confirm that the ZnO microspheres were actually hierarchical hollow structures, which are assembled from 2D nanosheets with a thickness of 40–50 nm. The typical TEM image in Fig. 1(e) shows a distinct hollow interior, where the size and shape of ZnO are similar to the observations from the FESEM. Fig. 1(f) presents the high resolution transmission electron microscopy (HRTEM) image and selected-area electron diffraction (SAED) pattern of the nanosheet labelled in Fig. 1(e) with a red rectangle. The interlayer spacings of 0.32 nm and 0.28 nm were determined and in good agreement with the *d*-spacings of the (010) and (100) planes for the

[a]*State Key Laboratory on Integrated Optoelectronics, College of Electronic Science and Engineering, Jilin University, Changchun 130012, China.*
E-mail: spmaster2008@163.com; lugy@jlu.edu.cn; Fax: +86 431 85167808; Tel: +86 431 85167808
[b]*State Key Laboratory of Luminescence and Application, Changchun Institute of Optics, Fine Mechanics and Physics, Chinese Academy of Sciences, Changchun 130033, China*

† Electronic supplementary information (ESI) available. See DOI: 10.1039/c3ce40812d

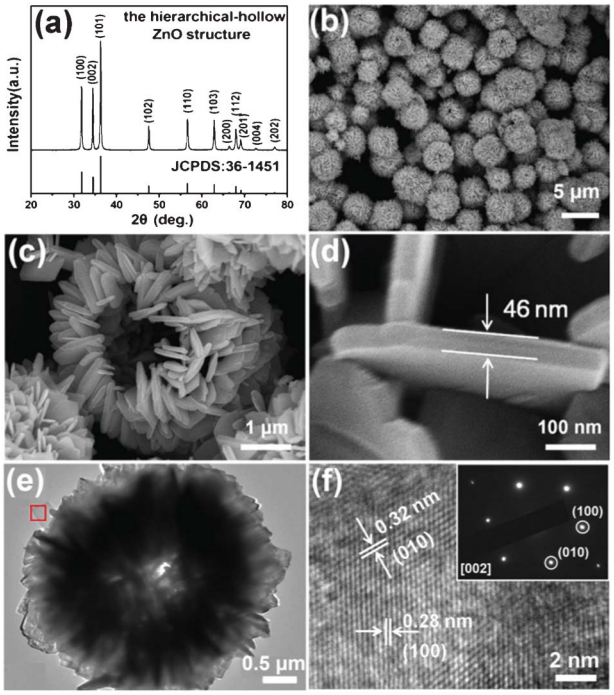

Fig. 1 (a) XRD pattern, (b–d) FESEM images, (e) TEM image and (f) HRTEM image of the hierarchical hollow ZnO microspheres (sample A, 0.05 M). The inset of (f) shows the corresponding SAED pattern.

hexagonal ZnO structure (JCPDS No. 36-1451). The crystalline planes (010) and (100) can also be identified in the SAED pattern, which indicate the single crystalline nature of the nanosheet and its main lattice plane is {002}.[17]

The influence of the zinc source concentration on the ZnO morphology was investigated by varying the concentration of zinc acetate between 0.05 M and 0.2 M, while keeping the other conditions constant. When the hydrothermal synthesis were carried out at a concentration of 0.05 M (designated as sample A), the hierarchical hollow ZnO microspheres were observed, as shown in Fig. 1(b)–(e). On increasing the concentration of zinc acetate to 0.1 M (designated as sample B), Fig. 2(a) and (b) show that the ZnO microspheres are still hollow structures. On continuing to increase the zinc source concentration to 0.2 M (designated as sample C), the FESEM image and TEM image in Fig. 2(c) and (d) show that the ZnO microspheres transformed into solid structures. The above results indicate that the hollowness of these ZnO microspheres can be controlled by adjusting the zinc source concentration. In addition, to investigate the effect of citrate anions on the ZnO morphology, a comparative experiment was carried out without tripotassium citrate monohydrate, while keeping the other conditions constant. The FESEM images in Fig. S2 (see the ESI†) show that the as-prepared products consist of monodispersed 2D nanosheets, with thicknesses of about 50 nm. It can be seen that citrate anions play a key role as an assembling agent on the formation of hierarchical hollow ZnO microspheres.

In order to further study the formation mechanism of the hierarchical hollow ZnO microspheres in this work, a series of experiments depending on different reaction times were performed, while maintaining the other hydrothermal conditions. The initial stage of the reaction mainly included the nucleation and aggregation process of ZnO tiny nanoparticles, as shown in Fig. 3(a) (see Fig. S3 in the ESI† for the low magnification). Following the Gibbs law,[18] in order to minimize the total surface energy, these nanoparticles further aggregated into nanosheets and these oriented ZnO nanosheets evolved into the 3D solid hierarchical microspheres through an oriented attachment, as shown in Fig. 3(b). When the hydrothermal synthesis was prolonged to 12 h, Fig. 3(c) shows that the solid ZnO microspheres transformed into hierarchical hollow structures. As the reaction time increased to 24 h, the hierarchical hollow ZnO microspheres collapsed gradually into littery nanosheets, as shown in Fig. 3(d). The main evolving steps are schematically illustrated in Fig. 3(e). This evolution of the morphology of the ZnO microspheres with the reaction time can be explained by the Ostwald ripening mechanism,[19–21] in which a classic phenomenon in particle growth involves the growth of larger particles at the cost of smaller particles due to the higher solubility of smaller particles.[22]

To investigate the sensing properties, sensors based on the as-prepared samples were fabricated, which were made by coating a paste onto an alumina tube with a pair of gold electrodes, as

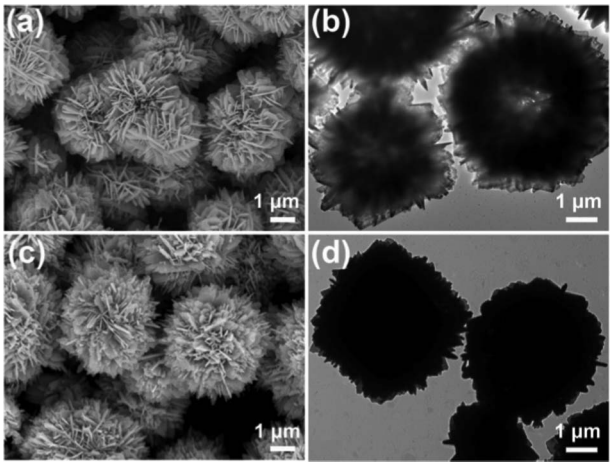

Fig. 2 FESEM and TEM images of the products prepared with different zinc source concentrations: (a) and (b) 0.1 M (sample B), (c) and (d) 0.2 M (sample C).

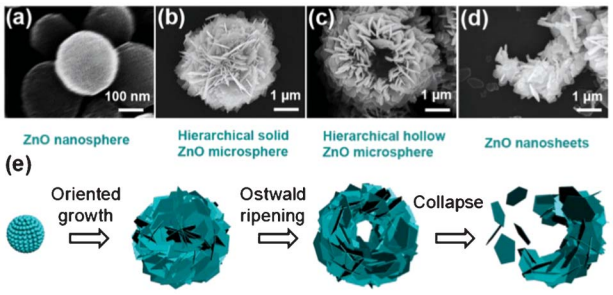

Fig. 3 FESEM images of the morphology evolution at different reaction times: (a) 0.5 h, (b) 3 h, (c) 12 h and (d) 24 h. (e) Schematic illustration of the formation process of the hierarchical hollow ZnO structure.

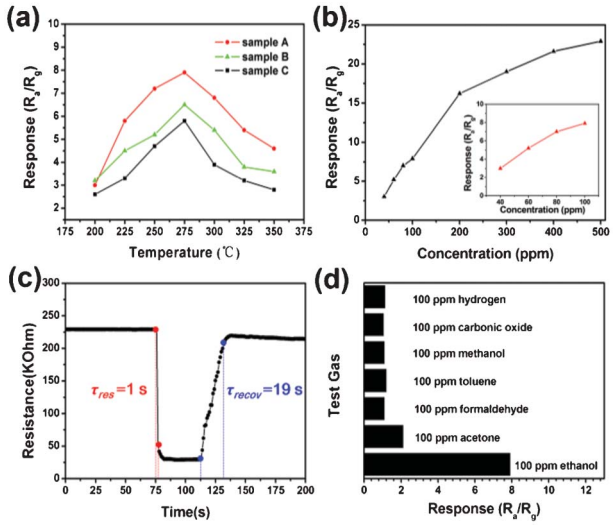

Fig. 4 (a) Response *versus* operating temperatures of the sensors based on sample A, B and C to 100 ppm ethanol; (b) response of the sensor based on sample A *versus* different ethanol concentrations at 275 °C (the inset shows the corresponding response *versus* the concentrations from 40 ppm to 100 ppm); (c) response transients of the sensor based on sample A to 100 ppm ethanol gas at 275 °C, τ_{res} and τ_{recov} stand for the response time and recovery time respectively; (d) comparison of the responses to various test gases at 275 °C (sample A).

shown in Fig. S1 (see the ESI† for more details). It is well known that the response of a gas sensor based on a semiconductor is highly influenced by the operating temperature.[23] To determine the optimum operating temperature, the response *versus* operating temperatures of the sensors based on sample A, B and C to 100 ppm ethanol were investigated first, as shown in Fig. 4(a). The response of the sensors increased up to 275 °C, then decreased gradually with further a increase of the operating temperature. It is obvious that the response of sample A is higher than those of sample B and C. The maximum responses were 8, 6.5 and 5.8 for sample A, B and C at 275 °C, respectively. The response *versus* different morphologies (for the samples grown at different reaction times: (a) 0.5 h, (b) 3 h, (c) 12 h and (d) 24 h) to 100 ppm ethanol at 275 °C were investigated, as shown in Fig. S4 (see the ESI†). Compared to other morphologies, the hierarchical hollow ZnO microspheres present a better response to ethanol. As an optimum, an operating temperature of 275 °C was chosen for the further investigation of the sensors based on hierarchical hollow ZnO microspheres.

Fig. 4(b) shows the response of the sensor based on sample A *versus* different ethanol concentrations at 275 °C. From the curve, it was found that the response increased with an increase of ethanol concentrations from 40 to 500 ppm. It can be seen that the responses were almost proportional to the increasing concentrations of ethanol when the concentrations were correspondingly low, as shown in the inset of Fig. 4(b). As the ethanol concentrations increased (above 200 ppm), the sensor tended to saturation gradually.

The response behavior and recovery behavior were investigated with the sensor based on sample A being exposed to 100 ppm ethanol at 275 °C, as depicted in Fig. 4(c). It can be seen that the sensor exhibited fast response and recovery, as revealed by the rapid changes in resistance, with a τ_{res} (response time) of 1 s and a τ_{recov} (recovery time) of 19 s, respectively. Compared to previous work,[5,24–30] the τ_{res} of hierarchical hollow ZnO microspheres to ethanol is much faster than those of other samples, and the τ_{recov} is also acceptable, as shown in Table 1.

Since selectivity is also an important parameter of gas sensors for their practical application, the selectivity of the sensor based on sample A was further investigated. Fig. 4(d) shows a comparison of responses to various test gases, including acetone, formaldehyde, toluene, methanol, carbonic oxide and hydrogen. All of the gases were tested at an operating temperature of 275 °C with an ethanol concentration of 100 ppm. As a result, the response of the sensor based on sample A was the highest compared to other test gases. This indicated that the hierarchical hollow ZnO structure exhibited a good selectivity to ethanol.

For ethanol gas sensing, the mechanism can be explained by the change in resistance caused by the chemical adsorption and reaction of gas molecules on the surface of the sensing material.[31] In air ambient, oxygen molecules are adsorbed onto the surface of the as-synthesized ZnO and generate the chemisorbed oxygen species (O_2^-, O^- and O^{2-}) by capturing electrons from the conduction band of ZnO. These chemisorbed oxygen species depend strongly on temperature. At low temperatures, O_2^- is commonly chemisorbed but at high temperatures, O^- and O^{2-} are commonly chemisorbed, while O_2^- disappears rapidly.[32] The reaction kinematics can be described as follows:[33]

Table 1 τ_{res} and τ_{recov} to ethanol for the ZnO sensors in this work and those reported in previous literature

ZnO morphology	Synthetic method	Ethanol (ppm)	T^c (°C)	$\tau_{res}{}^a$ (s)	$\tau_{recov}{}^b$ (s)	Ref.
ZnO nanorod arrays	Sol–gel method	100	300	~250	~130	24
ZnO nanorod	Hydrothermal method	100	320	47	50	25
ZnO nanowire	Evaporation	100	300	~20	~90	26
ZnO hollow microspheres	Precursor–template method	100	420	~20	~15	27
Porous ZnO spheres	Hydrothermal method	100	280	~11	~16	5
Al-doped ZnO nanomaterial	Thermal evaporation	3000	290	8	10	28
Porous ZnO nanosheets	Hydrothermal method	200	400	7	19	29
ZnO hierarchical nanostructures	Coprecipitation	50	400	4	357	30
Hierarchical hollow ZnO microspheres	Hydrothermal method	100	275	1	19	This work

[a] τ_{res}: response time. [b] τ_{recov}: recovery time. [c] T: sensor operating temperature.

$$O_2 + e^- \leftrightarrow O_2^- \quad (1)$$

$$O_2^- + e^- \leftrightarrow 2O^- \quad (2)$$

$$O^- + e^- \leftrightarrow O^{2-} \quad (3)$$

In this process, the resistance of the sensor increases. When the sensor is exposed to ethanol at a moderate temperature, the adsorbed oxygen species will react with these gas molecules on the ZnO surface. The reactions between ethanol and the chemisorbed oxygen species can be described as follows:[34]

$$C_2H_5OH + 3O_2^- \rightarrow 2CO_2 + 3H_2O + 3e^- \quad (4)$$

$$C_2H_5OH + 6O^- \rightarrow 2CO_2 + 3H_2O + 6e^- \quad (5)$$

$$C_2H_5OH + 6O^{2-} \rightarrow 2CO_2 + 3H_2O + 12e^- \quad (6)$$

As a result, the trapped electrons are released back to the conduction band of ZnO and the electron concentration increases, which leads to a decrease in the resistance of the sensor. From Fig. 4(d), it can be seen that hierarchical hollow ZnO structures displayed a good selectivity to ethanol. This may be attributed to the LUMO (lowest unoccupied molecule orbit) energy of ethanol. Compared to the other test gases, the LUMO energy for ethanol is lowest with a value of 0.12572 eV.[35] Therefore, the ability of capturing electrons and the possibility of electrons transferring between the gas molecules and the surface of the ZnO structures are best for ethanol. At the same operating temperature, the sensor exhibited an evident response to ethanol as its lower LUMO energy. In this work, the fast response–recovery performance to ethanol of the sensor should be attributed to the unique architecture of hierarchical hollow ZnO microspheres, which provide well-defined and well-aligned micro- and mesoporosity for effective gas diffusion. Compared to solid ZnO microspheres, the gas diffusion of hierarchical hollow ZnO microspheres is more effective and exhaustive because the gas can diffuse into the interior, which improves the utility factor of the sensing body. So, hierarchical hollow ZnO microspheres (sample A and B) present a better response than solid ZnO microspheres (sample C). The further gas sensing mechanism is still under investigation by our group.

In summary, we have successfully fabricated hierarchical hollow ZnO microspheres *via* a facile one-pot template-free hydrothermal synthesis, which were assembled from 2D nanosheets with a thickness of 40–50 nm. Interestingly, the hollowness of these microspheres could be tailored by adjusting the concentration of the zinc source (from 0.05 M to 0.2 M). On the basis of the experimental results, the Ostwald ripening mechanism was applied to understand the formation mechanism of the hierarchical hollow ZnO microspheres. At the same time, citrate anions play a key role as an assembling agent on the formation of hierarchical hollow ZnO microspheres. As for the potential applications, these microspheres exhibited a fast response time (1 s), fast recovery time (19 s) and good selectivity to ethanol. Compared to other morphologies, hierarchical hollow ZnO microspheres present a better response to ethanol due to their unique architectures.

This work was supported by the Natural Science Foundation of China (61074172, 61134010), the Program for Changjiang Scholars and Innovative Research Team in University (No. IRT1017), the State "863" project (2013AA030902), the China Ministry of Public Security (No. 2011ZDYJJLST010) and the project (20121105) supported by the Graduate Innovation Fund of Jilin University.

Notes and references

1 J. H. Lee, *Sens. Actuators, B*, 2009, **140**, 319.
2 J. Hu, M. Chen, X. Fang and L. Wu, *Chem. Soc. Rev.*, 2011, **40**, 5472.
3 M. Huang, S. Mao, H. Feick, H. Yan, Y. Wu, H. Kind, E. Weber, R. Russo and P. Yang, *Science*, 2001, **292**, 1897.
4 N. Saito and H. Haneda, *Sci. Technol. Adv. Mater.*, 2011, **12**, 064707.
5 W. Wang, Y. Tian, X. Wang, H. He, Y. Xu, C. He and X. Li, *J. Mater. Sci.*, 2013, **48**, 3232.
6 H. Wang, L. Xin, H. Wang, X. Yu, Y. Liu, X. Zhou and B. Li, *RSC Adv.*, 2013, **3**, 6538.
7 X. D. Wang, J. Zhou, J. H. Song, J. Liu, N. Xu and Z. L. Wang, *Nano Lett.*, 2006, **6**, 2768.
8 P. D. Yang, H. Q. Yan, S. Mao, R. Russo, J. Johnson, R. Saykally, N. Morris, J. Pham, R. He and H. J. Choi, *Adv. Funct. Mater.*, 2002, **12**, 323.
9 M. Law, L. E. Greene, J. C. Johnson, R. Saykally and P. D. Yang, *Nat. Mater.*, 2005, **4**, 455.
10 S. C. Navale, S. W. Gosavi and I. S. Mulla, *Talanta*, 2008, **75**, 1315.
11 Ü. Özgür, Y. L. Alivov, C. Liu, A. Teke, M. A. Reshchikov, V. Avrutin, S. J. Cho and H. Morkoc, *J. Appl. Phys.*, 2005, **98**, 041301.
12 D. C. Look, *Mater. Sci. Eng., B*, 2001, **80**, 383.
13 B. Ismail, M. A. Abaab and B. Rezig, *Thin Solid Films*, 2001, **383**, 92.
14 O. Lupan, L. Chow, T. Pauporté, L. K. Ono, B. R. Cuenya and G. Chai, *Sens. Actuators, B*, 2012, **173**, 772.
15 J. Zhang, S. Wang, Y. Wang, M. Xu, H. Xia, S. Zhang, W. Huang, X. Guo and S. Wu, *Sens. Actuators, B*, 2009, **139**, 411.
16 Y. Tian, J. Li, H. Xiong and J. Dai, *Appl. Surf. Sci.*, 2012, **258**, 8431.
17 K. X. Yao and H. C. Zeng, *J. Phys. Chem. B*, 2006, **110**, 14736.
18 P. Sun, W. Zhao, Y. Cao, Y. Guan, Y. Sun and G. Lu, *CrystEngComm*, 2011, **13**, 3718.
19 T. L. Sounart, J. Liu, J. A. Voigt, M. Huo, E. D. Spoerke and B. McKenzie, *J. Am. Chem. Soc.*, 2007, **129**, 15786.
20 D. F. Zhang, L. D. Sun, J. L. Yin, C. H. Yan and R. M. Wang, *J. Phys. Chem. B*, 2005, **109**, 8786.
21 R. Bardhan, H. Wang, F. Tam and N. J. Halas, *Langmuir*, 2007, **23**, 5843.
22 W. Z. Ostwald, *Phys. Chem.*, 1897, **22**, 289.
23 Z. Cao and J. R. Stetter, *Sens. Actuators, B*, 1991, **5**, 109.
24 C. M. Chang, M. H. Hon and I. C. Leu, *Sens. Actuators, B*, 2010, **151**, 15.
25 L. Wang, Y. Kang, X. Liu, S. Zhang, W. Huang and S. Wang, *Sens. Actuators, B*, 2012, **162**, 237.
26 T. J. Hsueh, C. L. Hsu, S. J. Chang and I. C. Chen, *Sens. Actuators, B*, 2007, **126**, 473.

27 Y. Tian, J. Li, H. Xiong and J. Dai, *Appl. Surf. Sci.*, 2012, **258**, 8431.
28 Z. Yang, Y. Huang, G. Chen, Z. Guo, S. Cheng and S. Huang, *Sens. Actuators, B*, 2009, **140**, 549.
29 L. Zhang, J. Zhao, H. Lu, L. Li, J. Zheng, H. Li and Z. Zhu, *Sens. Actuators, B*, 2012, **161**, 209.
30 K. M. Kim, H. R. Kim, K. I. Choi, H. J. Kim and J. H. Lee, *Sens. Actuators, B*, 2011, **155**, 745.
31 N. Yamazoe, *Sens. Actuators, B*, 1991, **5**, 7.
32 J. C. Belmonte, J. Manzano, J. Arbiol, A. Cirera, J. Puigcorbé, A. Vilà, N. Sabaté, I. Gràcia, C. Cané and J. R. Morante, *Sens. Actuators, B*, 2006, **114**, 881.
33 P. P. Sahay, *J. Mater. Sci.*, 2005, **40**, 4383.
34 T. Gao and T. H. Wang, *Appl. Phys. A: Mater. Sci. Process.*, 2005, **80**, 1451.
35 W. Zeng and T. M. Liu, *Phys. B*, 2010, **405**, 1345.

